ELSEVIER

PII: S0144-8617(96)00084-7

Carbohydrate Polymers **30** (1996) 77–81

0144-8617/96/$15.00 + .00

Observation of gellan gum by scanning tunneling microscopy

K. Nakajima, T. Ikehara & T. Nishi

Department of Applied Physics, Faculty of Engineering, The University of Tokyo, Bunkyo, Tokyo 113, Japan

A bacterial polysaccharide, gellan gum, was deposited on highly oriented pyrolytic graphite and was studied by means of scanning tunneling microscopy. The sample was prepared in the presence of cations to make double helices of gellan associate into cation-mediated aggregates. This study is the first direct confirmation of the helix structure of gellan in the real space. An image of a cross-linking domain, observed in the ambient condition, showed that half a pitch of the double helix was *ca* 2.6nm and that the separation of strands was *ca* 2.3nm. The effect of co-existing cations on the strength of macroscopic gels was discussed in relation to the microscopic structures observed by STM. The difference of cations mainly influenced the length of strands of gellan. Copyright © 1996 Elsevier Science Ltd

INTRODUCTION

Gellan gum is a deacylated form of extracellular bacterial polysaccharide from *Pseudomonas elodea*. It is widely used in the food industry and in biotechnology because it forms a transparent gel which is heat resistant and its strength is less dependent on pH in comparison with other polysaccharide gels. Jansson *et al.* (1983) established that the chemical structure has a tetrasaccharide repeating sequence, →3)-β-D-Glcp-(1→4)-β-D-GlcpA-(1→4)-β-D-Glcp-(1→4)-α-L-Rhap-(1→, as shown in Fig. 1.

The thermoreversible sol–gel transition controlled by temperature and ionic strength was first related to a conformational transition by Crescenzi *et al.* (1987), and was investigated using various techniques (optical rotation, light scattering, viscosity, conductivity) by Milas *et al.* (1990). They concluded that this conformational transition was in agreement with a two-coil–one-double-helix transition. Chandrasekaran *et al.* (1988a, b) and Chandrasekaran & Thailambal (1990) confirmed the existence of a double-helix structure from X-ray crystallographic studies of polycrystalline and well-oriented samples of lithium (Chandrasekara *et al.*, 1988a) , potassium (1988b), and calcium (1990) salts of gellan. In the solid state, this polysaccharide adopts a double helix structure with two left-handed, three-fold chains, each of which is translated by half a pitch ($p = 5.63$nm) with respect to the other. This arrangement is similar to the double helix structure of ι-carrageenan (Arnott *et al.*, 1974).

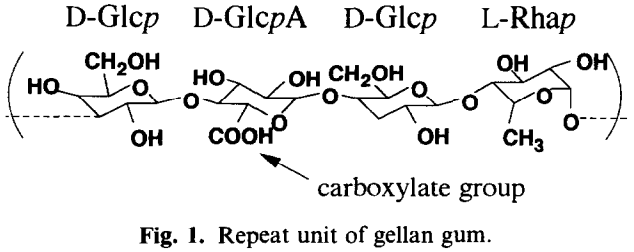

Fig. 1. Repeat unit of gellan gum.

Although gellan without any salts forms only weak gels (Moorhouse, 1987), it forms strong gels in the presence of moderate concentrations (>60mM) of monovalent ions, such as sodium or potassium, or of much lower concentrations of divalent ones, typically calcium (Robinson *et al.*, 1991). A suggested mechanism for gelation is as follows. At high temperature, gellan in solution is in the coil form; below the gel point T_m (*ca* 35°C), in the presence of appropriate cations, the helices associate into cation-mediated aggregates which serve as cross-linking points (Fig. 2), where double helix–monovalent, ion–water–monovalent, ion–double helix interaction plays a dominant role for gel stabilization. The proportion of aggregated helices increases with salt concentration. The effect of these monovalent cations associating with carboxylate groups in every tetrasaccharide repeating-unit on the promotion of strong gelation is due to the screening of the electrostatic repulsion between the ionized carboxylate groups. The strong interactions in the double helix–calcium, ion–double helix cross-links were also proposed (Chandrasekaran & Thailambal, 1990).

In this study, we observed thin films of gellan gum with several kinds of salts (including gellan gum without

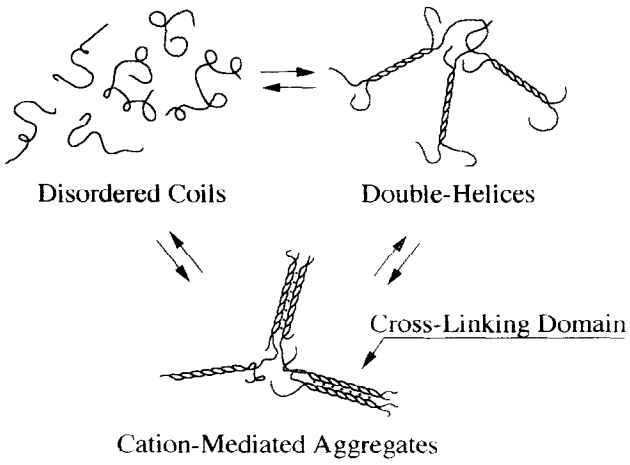

Fig. 2. Schematic representation of a predicted model for the conformation and functional interaction of gellan, showing the processes envisaged on cooling and heating both in the presence and the absence of cations. One monovalent cation associates with a carboxylate group in every tetrasaccharide repeating-unit.

any salts) deposited on highly oriented pyrolytic graphite (HOPG) by means of scanning tunneling microscopy (STM). The structure of a cross-linking domain of K^+–gellan was directly visualized for the first time and the pitch measured by this method was compared with that determined by X-ray diffraction study. The effect of co-existing cations on the strengths of macroscopic gels will be also discussed in relation to the microscopic structures observed by STM.

EXPERIMENTAL

Commercial samples of gellan gum were supplied by Dr G.R. Sanderson (Kelco Division of Merck & Co., Inc., San Diego, CA). The results of inductively coupled plasma spectrometry (ICP) are summarized in Table 1. Two types of gellan were prepared: one contained mainly K^+ (sample 1), and the other contained larger amounts of Na^+ than K^+ (sample 2). The latter can be solubilized even in cold water. For sample 1, an aqueous solution (0.46wt%) was stirred above 80°C and held there for 20min to solubilize the gum. An appropriate amount of KCl was added to the agitated solution and kept at 90°C for 10min. The K^+ concentration of this solution (113mM) was sufficient for strong gelation after cooling below the gel point T_m. Note that the present concentration is higher than the threshold for gelation (~60mM). In addition, sample 2 was used to study the effect of co-existing cations. Four aqueous solutions were prepared as shown in Table 2. All of these solutions contain the same amount of gellan (0.50wt%). The salt concentrations were 120mM for monovalent ions (sodium, potassium), and 25mM for divalent ion (calcium). The gel properties are also summarized in Table 2.

STM samples were prepared as follows: (1) deposition of the hot aqueous solution of gellan onto a freshly cleaved HOPG substrate followed by immediate spin-coating at 2500~4000rpm for 60s, (2) left as it was for 1h for drying. In the absence of rotation, gelation was completed within 1s. We therefore concluded that gellan near the HOPG substrate had already undergone gelation while spin-coating, and a gel rather than a solution structure was observed. Film thickness was controlled by the rate of spin-coating. The sample which was prepared using sample 1 (thick film of K^+–gellan) was thicker than those using sample 2 (thin films of Na^+, K^+, Ca^{2+}–gellan and thin film of gellan without salt).

The STM used was Nanoscope II (Digital Instruments, Inc., Santa Barbara, CA). Observation was performed in air at room temperature with a special scanner (large-scale imaging purpose: $12\times12\mu m^2$ max.) for the thick film of K^+–gellan and with a common scanner (atomic-scale imaging purpose: $480\times480nm^2$ max.) for other samples. In order to insure that the obtained images represented the correct corrugations of surfaces, we took an image of an HOPG surface with the same Pt–Ir tip before observation of the thin films of gellan. All STM images were obtained in the constant current mode, i.e. a constant tip–sample distance, at various scan rates (4.3–78.1Hz). All of the images are raw unprocessed data without slight low-pass filtering.

Table 1. The results of ICP spectrometry for two types of gellan

	Na^+	K^+	Ca^{2+}	Mg^{2+}
Sample 1	0.19%	2.08%	0.51%	0.51%
Sample 2	3.03%	0.19%	0.11%	0.02%

RESULTS AND DISCUSSION

Thick film of K^+–gellan

An STM image of the gellan film on a cleaved HOPG substrate is shown in Fig. 3(a). The scan size, the bias voltage, and the tunneling current were $284.6\times284.6nm^2$, −1.0V, and 0.50nA, respectively. The

Table 2. The gel properties of four macroscopic gels made of sample 2

	Color	Strength
Gellan without salt	transparent	weak
Na^+–gellan	transparent	thixotropic
K^+–gellan	transparent	strong
Ca^{2+}–gellan	cloudy (inhomogeneous)	very strong*

*This gel did not return to the sol state reversibly up to 100°C.

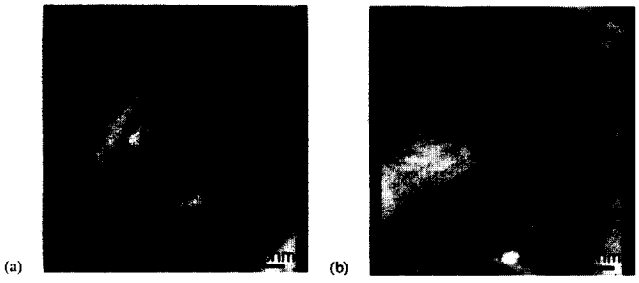

Fig. 3. (a) STM top view image of the thick film of K^+-gellan on a HOPG substrate. The scan size, the biased voltage, and the tunneling current are $284.6 \times 284.6 nm^2$, $-1.0V$, and 0.50nA, respectively. Scan rate is 4.3Hz. (b) The magnified image of (a). Scan size is $60.1 \times 60.1 nm^2$. The biased voltage and the tunneling current are the same as those for Fig. 3 (a). Scan rate is faster (78.1Hz) than before. The cross-linking domain can be observed in the middle of this image. There exist other strands, which are indicated by the arrows.

scan rate was slow at 4.3Hz in case the tip should collide with the uneven sample. The image clearly shows gellan aggregates covering the substrate. Their average height is *ca* 16nm, indicating that this film does not behave as an insulator. An insulator whose thickness is larger than *ca* 1nm cannot be observed by STM. The fact that each repeating-unit has a carboxylate group and that this polysaccharide is therefore a weak polyelectrolyte may be related to the conducting mechanism. In addition, they cannot be artifacts produced by flakes of HOPG substrate as reported by Clemmer and Beebe (1991) because of the manner of aggregation. On the right side of this image near the bare HOPG, some strands lie diagonally from the lower left to the upper right. They should be the cross-linking domains described in Fig. 2.

In order to inspect the structures of these strands in detail, we magnified it as shown in Fig. 3(b). The scan size and rate were $60.1 \times 60.1 nm^2$ and 78.1Hz, respectively, while the bias voltage and the tunneling current were unchanged. Three distinct rows with bright spots run parallel to each other in the middle of this STM image.

Fast Fourier Transform (FFT) taken along the center row reveals the periodicity along the rows is 2.59nm, while an X-ray diffraction study by Chandrasekaran *et al.* (1988a, b) revealed that half a pitch was 2.815nm. The discrepancy (8% accuracy) between these values is slightly large for the consensus in the scanning probe community. However, it can be attributed to hysteresis of the large-scale piezo-electric scanner and to thermal drift of the instrument which is affected by the degree of scan rate. After taking several dozens of STM images with other tips and scanners and conducting statistical analysis, the average periodicity along rows became *ca* 2.7nm (4% accuracy). This value is also slightly smaller than that obtained from X-ray crystallographic study. These results were obtained with solid-state gellan, whereas our samples were in the gel-state. This difference may explain this small contradiction. Although there is this discrepancy in the periodicity along the gellan strands, we can conclude from structural consideration that a row containing bright spots can be assigned to one double-helical strand, and the three rows parallel with each other correspond to cation-mediated aggregate which form the gel network (cross-linking domain). Strictly speaking, STM images cannot be interpreted as simple topological maps of the surface without regard to the complex nature of STM imaging. A more detailed experiment is needed for this purpose because of the lack of higher resolution.

On the upper and lower left sides of this image, some other strands lie on the substrate. There is also another strand parallel with the cross-linking domain. These strands are indicated by the arrows in Fig. 3(b). Although we could not observe clear periodicity because of the larger distances from the STM tip compared with the cross-linking domain existing in the middle of this image (1.9–2.5nm lower) and the faster scan rate than that previously used in imaging Fig. 3(a), these strands are considered to be the double-helices and contribute to the gel network together with the cross-linking domain.

Figure 4 shows a cross-sectional profile perpendicular to the strand axis for Fig. 3(b). The corresponding portion is drawn by the solid line in Fig. 3(b). The separation of strands, which are indicated by arrows, is 2.32nm. In the solid state, two duplexes of gellan are reported (Chandrasekaran *et al.*, 1988a, b) to exist in a trigonal unit cell, where $a = b = 1.575$nm, and $c = 2.815$nm (corresponding to periodicity along the strand axis). Compared with this structure, the value of 2.32nm for the distance between two strands is larger. This probably indicates that cross-linking domains of the cast film of gellan on the substrate are loosely packed because of an interaction with HOPG and/or the presence of solvent in the initial gel disposed on the substrate before drying. The factors previously used to explain the discrepancy in pitches would also be significant. However, the separation becomes much larger after calibration by the ratio of the pitch in this study (2.59nm) to the crystallographic value (2.815nm).

According to a small-angle X-ray scattering study (Yuguchi *et al.*, 1993), gellan in solution (gel state) shows dimer, trimer, and higher order associations. As shown in Fig. 4, the aggregate with three strands on the top of itself has a height of *ca* 9nm from the substrate. Though it cannot be an aggregate as a whole in solution, a part of it is possibly assigned to the higher order association which promotes gelation.

The effect of co-existing cations

STM images of thin films of gellan without any salt, and with sodium, potassium and calcium salts on cleaved

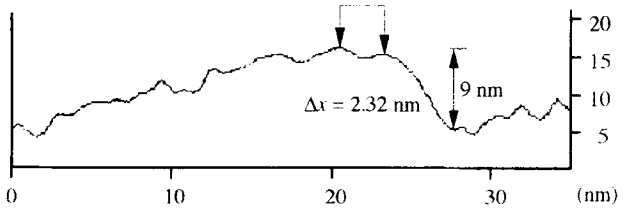

Fig. 4. A cross-sectional profile perpendicular to the strand axis for Fig. 4. The separation between two strands is 2.32nm.

HOPG substrates are shown in Fig. 5(a–d), respectively. The scan size of these images is identical with each other, $84.5 \times 84.5 nm^2$. The bias voltage, the tunneling current, and the scan rate. Though only low resolution had been attained in Fig. 5(a), it can be seen that aggregates consisting of gellan strands lie sparsely on the HOPG substrates in Fig. 5(b–d). Note that the scan rates in preparing these samples were somewhat faster than those used in obtaining the micrographs shown in Fig. 3.

Figure 6 shows a cross-sectional profile whose corresponding portion is drawn by the solid line in Fig. 5(c). As indicated by the arrow, the left projection can be regarded as a dimer of double-helix of K^+-gellan. Δz, which is equals to 0.51nm, is almost the same as the diameter of the double-helix. The right projection, on the other hand, can be assigned to a higher order association whose height is about twice that of the left one (1.22nm). Here can we confirm the existence of higher order association of the gellan double-helix again.

Comparing the four STM images with each other, we might conclude that the difference of co-existing cations mainly influences the length of the gellan strands. The average strand length of four types of gellan (corresponding to Fig. 5(a–d)) is summarized in Table 3. This averaging was conducted by measuring several dozens of strands for each type of gellan. From Table 3, it is observed that the strand length of gellan increases in the order: no salt $< Na^+ < K^+ < Ca^{2+}$. In addition, we know the strength of macroscopic gels forms the same sequence from Table 2, implying that these quantities have a certain relationship between each other. Extremely long associations with lengths > 120nm were observed in the case of Ca^{2+}-gellan. This may indicate the strong and stiff connections between strands bridged by divalent cations as reported by Chandrasekaran & Thailambal (1990).

It is natural for the strand length to be associated with the number of connected links, corresponding to double helix–monovalent ion–water–monovalent ion double helix interaction, as described in Fig. 7. In this

Table 3. The average strand length of four types of gellan

	The average strand length (nm)
Gellan without salt	17
Na^+-gellan	30
K^+-gellan	40
Ca^{2+}-gellan	70 <

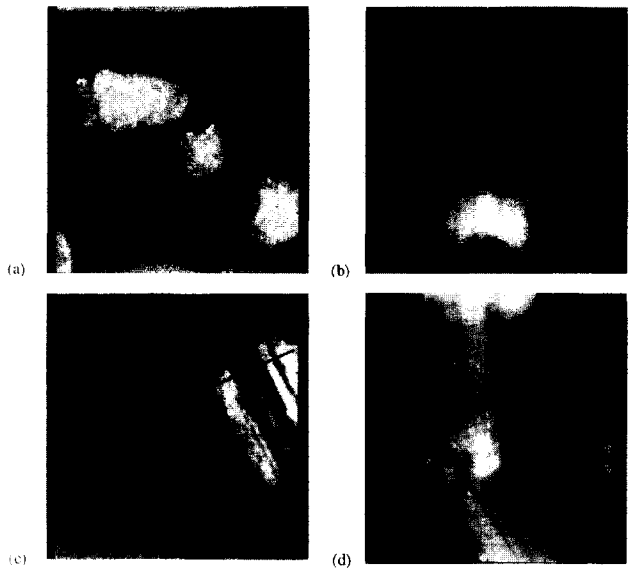

Fig. 5. STM images of thin films of gellan with several kinds of salt on cleaved HOPG substrates Values given are bias voltage, tunnel current and scan rate, respectively. (a) Gellan without any salt, −0.4V, 2.10nA, 8.7Hz. (b) Gellan with sodium salt, −1.0V, 4.36nA, 8.7Hz. (c) Gellan with potassium salt, −1.5V, 4.95nA, 31.3Hz. (d) Gellan with calcium salt, 1.0V, 1.00nA, 4.3Hz. The scan size of these images is identical with each other, $84.5 \times 84.5 nm^2$.

context, a simple estimation of the effect of ionic strength on the strand length can be established using a well-known zipper model (Nishinari *et al.*, 1990).

Using the partition function of the zipper model,

$$Z = \sum_{p=0}^{N-1}(p+1)G^p \exp(-p\varepsilon/\tau) = \sum_{p=0}^{N-1}(p+1)x^p, (x \equiv G\exp(-p\varepsilon/\tau)) \quad (1)$$

we can obtain the average number of links which have already opened,

$$\langle p \rangle = \sum_{p=0}^{N-1} p(p+1)x^p = \frac{x[2 - N(N+1)x^{N-1} + 2(N^2-1)x^N - N(N-1)x^{N+1}]}{[1-(N+1)x^N + Nx^{N+1}](1-x)}. \quad (2)$$

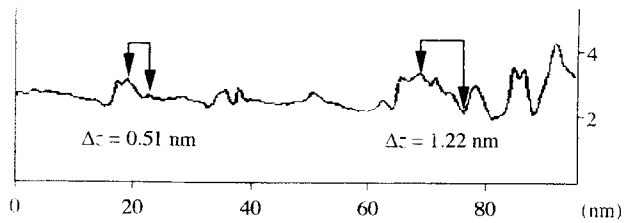

Fig. 6. A cross-sectional profile for Fig. 5 (c). Both dimer and higher order association of the double-helix of K^+-gellan are indicated by the arrows.

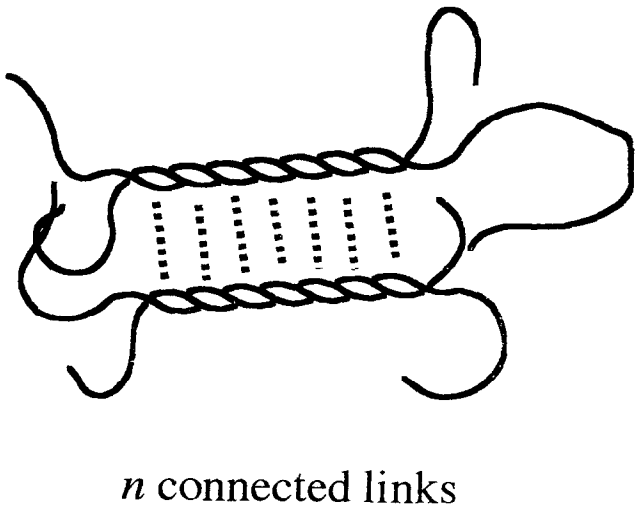

Fig. 7. Schematic representation of double helix–monovalent ion–water–monovalent ion–double helix interaction as a connected link (zipper model).

where p is the number of open links, N is the maximum number of zipper links, G is the number of orientations which an open link can take, e is the bonding energy, and $\tau = k_B T$ (k_B: the Boltzmann constant). Assuming e is sufficiently smaller than t, i.e., since the quantity e is the bonding energy, weak connection is assumed, $\langle n \rangle = N - \langle p \rangle$, the average number of connected links can be obtained by

$$\langle n \rangle = N - \langle p \rangle \approx \frac{N}{x} = \frac{N}{G}\exp\left(\frac{\varepsilon}{\tau}\right) \approx \frac{N}{G}\left(1 + \frac{\varepsilon}{\tau}\right). \qquad (3)$$

$\langle n \rangle$ is proportional to ε. Consequently, the strand length is proportional to e, giving the starting point of explaining the relationship between macroscopic strength of gel and the type of co-existing cation.

Our emphasis can be put on the above-mentioned assumption. As the strand length is of the order of 10nm, the number of connected (not opening) links becomes at most 20~40, therefore the connections are weak. Beside the above discussion, the macroscopic strength of gellan gel is thought to have a certain relationship not only with the length of strand but also with the manner of aggregation, i.e. the number of strands which are contained in an aggregate. It is expected that the greater the number of strands, the stronger the macroscopic gel becomes. A more detailed experiment and a sophisticated model are needed in order to clarify this relationship.

CONCLUSIONS

Double-helix structure of gellan associating into cation-mediated aggregates was observed for K^+–gellan using scanning tunneling microscopy. The arrangement of strands in an aggregate was altered by the interaction between HOPG and the thin film of gellan and by the presence of solvent in the initial gel disposed on the substrate before drying. Different cations influence the length of strands of gellan. In a zipper model, this length corresponds to the number of links and relates to the strength of macroscopic gel.

ACKNOWLEDGEMENTS

We are very grateful to Prof. Nishinari of Faculty of Human Life Science, Osaka City University for sending us a gellan gum sample from Kelco and some references related to the structure of gellan gum.

REFERENCES

Arnott, S., Scott, W.E., Rees, D.A. & McNab, C.G.A. (1974). *J. Mol. Biol.*, **90,** 253–267.

Chandrasekaran, R., Millane, R.P., Arnott, S. & Atokins, E.D.T. (1988a). *Carbohydr. Res.*, **175,** 1–15.

Chandrasekaran, R., Puigjaner, L.C., Joyce, K.L. & Arnott, S. (1988b). *Carbohydr. Res.*, **181,** 23–40.

Chandrasekaran, R. & Thailambal, V.G. (1990). *Carbohydr. Polym.*, **12,** 431–442.

Clemmer, C.R. & Beebe, T.P.Jr (1991). *Science,* **251,** 640–642.

Crescenzi, V., Dentini, M. & Dea, I.C.M. (1987). *Carbohydr. Res.*, **160,** 283–302.

Jansson, P.E., Lindberg, B. & Sandford, P.A. (1983). *Carbohydr. Res.*, **124,** 135–139.

Milas, M., Shi, X. & Rinaudo, M. (1990). *Biopolymers,* **30,** 451 464.

Moorhouse, R. (1987). In *Industrial Polysaccharides: Genetic Engineering, Structire/Property Relations and Applications*, ed. M. Yalpani, Elsevier Science Publishers, Amsterdam, pp. 187–206.

Nishinari, K., Koide, S., Williams, P.A. & Phillips, G.O. (1990). *J. Phys. (France),* **51,** 1759–1768.

Robinson, G., Manning, C. E. & Morris, E. R. (1991). In *Food Polymers, Gels, and Colloids*, ed. E. Dickinson, Roy. Soc. Chem., UK, pp. 22–33.

Yuguchi, Y., Miura, M., Urakawa, H., Kajiwara, K., Kitamura, S. & Ohno, S. (1993). *Polym. Prepr. Jpn.*, **42,** 3006–3008.